World Electric Vehicle Journal

MDPI

Article

Experimental Investigation on Affecting Air Flow against the Maximum Temperature Difference of a Lithium-Ion Battery with Heat Pipe Cooling

Chokchai Anamtawach [1], Soontorn Odngam [2] and Chaiyut Sumpavakup [2,*]

[1] Department of Power Engineering Technology, College of Industrial Technology, King Mongkut's University of Technology North Bangkok, Bangkok 10800, Thailand; s6103026911516@email.kmutnb.ac.th
[2] Research Centre for Combustion Technology and Alternative Energy—CTAE, College of Industrial Technology, King Mongkut's University of Technology North Bangkok, Bangkok 10800, Thailand; soontorn.o@cit.kmutnb.ac.th
* Correspondence: chaiyut.s@cit.kmutnb.ac.th

Abstract: Research on battery thermal management systems (BTMSs) is particularly significant since the electric vehicle sector is growing in importance and because the batteries that power them have high operating temperature requirements. Among them, heat pipe (HP)-based battery thermal management systems have very high heat transfer performance but fall short in maintaining uniform temperature distribution. This study presented forced air cooling by an axial fan as a method of improving the cooling performance of flat heat pipes coupled with aluminum fins (FHPAFs) and investigated the impact of air velocity on the battery pack's maximum temperature differential (ΔT_{max}). All experiments were conducted on lithium nickel manganese cobalt oxide (NMC) pouch battery cells with a 20 Ah capacity in seven series connections at room temperature, under forced and natural convection, at various air velocity values (12.7 m/s, 9.5 m/s, and 6.3 m/s), and with 1C, 2C, 3C, and 4C discharge rates. The results indicated that at the same air velocity, increasing the discharge rate increases the ΔT_{max} significantly. Forced convection has a higher ΔT_{max} than natural convection. The ΔT_{max} was reduced when the air velocity was increased during forced convection.

Keywords: battery thermal management system; lithium-ion battery; heat pipe; cooling performance; air flow; electric vehicle; maximum temperature differential; convection

Citation: Anamtawach, C.; Odngam, S.; Sumpavakup, C. Experimental Investigation on Affecting Air Flow against the Maximum Temperature Difference of a Lithium-Ion Battery with Heat Pipe Cooling. *World Electr. Veh. J.* **2023**, *14*, 306. https://doi.org/10.3390/wevj14110306

Academic Editors: Andrew F. Burke, Jingyuan Zhao and Jinrui Nan

Received: 9 October 2023
Revised: 31 October 2023
Accepted: 4 November 2023
Published: 7 November 2023

1. Introduction

At present, the trend of sustainability is popular in many countries. Due to the United Nations Framework Convention on Climate Change (UNFCCC) Conference of the Parties 26 (COP26) in Glasgow, United Kingdom, from 31 October–13 November 2021 [1], Thailand attended this meeting and announced its policy to reach carbon neutrality by 2050 and net-zero greenhouse gas emissions (GHG) before 2065 [2]. The COP26 meeting motivated the governance department to set the policy for green energy and emission reduction in Thailand. The Electric Vehicle Association of Thailand, or EVAT, is the organization that promotes and supports the industrial manufacturing, research, and development of electric vehicles in Thailand. EVAT recorded the status number of new electric vehicle (EV) registrations in Thailand, and the result shows an increasing number of vehicles, such as battery electric vehicles (BEV), plug-in hybrid electric vehicles (PHEV), and hybrid electric vehicles (HEV), from 2018 to 2022 [3], as shown in Figure 1.

The growth in electric vehicles is the best way to reduce emissions, provide clean energy for transportation, and be environmentally friendly. Other advanced energy conversion technologies, such as thermoelectric, can advance the development of environmentally friendly transportation [4]. The most common power source in an electric

vehicle is a lithium-ion battery (LIB) because of its high power, low self-discharge, favorable stability, and long life cycle [5]. There are many kinds of LIB, such as lithium iron phosphate (LFP), NMC, lithium nickel cobalt aluminum oxide (NCA), lithium-ion manganese oxide (LMO), lithium-ion cobalt oxide (LCO), lithium titanium oxide (LTO), etc. Numerous research studies have proposed methods to enhance the efficiency of lithium-ion batteries [6,7]. However, excessive temperatures have been shown to have the following effects: lithium melting, capacity decay, power attenuation, self-discharge, and thermal runaway [8]. Many studies propose improved approaches to advanced battery safety management with machine learning (ML) in battery fire diagnosis and early warning [9]. In general, when the battery temperature is too high, the stability, safety, and service lifetime are all affected [10]. Hence, it is important to monitor the health status of lithium batteries during operation. The micro-health parameters stand for the performance of active material and electrolytes inside the battery, and changes in the micro-health parameters can represent the battery's internal health state [11]. The ideal electrochemical performance of Li-ion batteries is between 25 °C and 40 °C with a maximum 5 °C temperature difference within the module or pack [12]. Designing a functional BTMS can ensure the safe operation of Li-ion batteries because heat generation by Li-ion batteries is an inevitable phenomenon. The primary classifications of BTMSs are based on their power requirements, heat transfer medium, and contact between the coolant and the battery surface [13]. Additionally, a battery pack's cell configuration can be used to categorize it [14]. However, the cooling techniques can be divided into two groups: traditional BTMSs and new BTMSs. Air, liquid, and refrigerant were used in traditional BTMSs, and a heat pipe, PCM, and thermoelectric elements were used in new BTMSs [15].

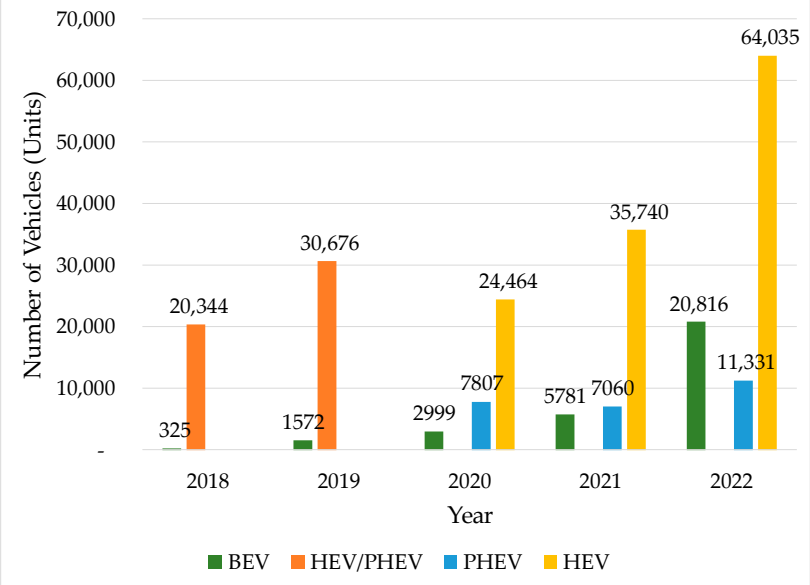

Figure 1. Number of new EV registrations in Thailand [3].

Air cooling can be classified as free or forced convection cooling [16]. The main benefits of these systems include their affordability, electrical safety, low weight, lack of leakage concerns, ease of maintenance, and others [17]. Natural cooling proved insufficient to meet the demands of a high-temperature working environment, bigger battery pack cooling, and high charge–discharge cycles. The forced-air cooling method is used in conjunction with the addition of exhaust fans [18,19], blowers [20], redesigned airflow channels [21], fin structures [22], etc., to overcome these constraints.

Phase change materials (PCMs) are used in the passive thermal management system known as PCM-BTMS. Because PCMs absorb a lot of heat through latent heat without

changing their temperature, they are suitable for passive battery thermal management. Additionally, the battery pack can be kept at the ideal temperature by adjusting the phase change temperature of PCMs [23]. Because of their low cost, simple installation, and excellent cooling efficiency, PCM-based battery thermal management systems are regarded as the most promising cooling technology among all BTMSs. The uniform distribution of the cell surface temperature is another outstanding and significant benefit of PCM-BTMSs. The usage of PCM-BTMSs has been hampered by low heat conductivity, leakage, and the occurrence of volume changes in pure PCMs, and numerous investigations are being conducted to address these problems [24].

The heat pipe is a heat transfer component with extremely high thermal conductivity that transfers heat through the evaporation and condensation of a working fluid in a completely enclosed vacuum tube that is primarily separated into two parts: the evaporator and condenser. Additionally, many heat pipes have an adiabatic component that performs the transport function and separates the evaporator and condenser at the proper distance to meet heat pipe usage criteria. A heat pipe may have more than one evaporator, condenser, and transport section. The fundamental idea behind a heat pipe is to transport heat through capillary action. This method has a number of benefits, including high thermal conductivity, isothermal, variability, reversibility, qualities that maintain a constant temperature, and environmental adaptability. According to their shapes, heat pipes can be categorized into numerous types, including loop heat pipes, oscillating heat pipes, flat heat pipes, and tubular heat pipes [25]. The advantages of such a system are its high heat transfer rate, low weight, small size, low cost, extended lifespan, and great capacity for transferring heat from the interior of the battery pack to the outside [26]. To guarantee optimal performance, the heat pipe construction in the condenser portion can also be combined with forced air [27], a water spray [28], or a PCM [29]. To increase the rate of heat transfer, some researchers have attached an aluminum fin to the condenser [30]. With an HP-BTMS, it is still difficult to keep the battery temperature within the optimal range, especially when the charge–discharge rate is high. Some studies have used plate-flat heat pipes for BTMSs to achieve temperature homogeneity in the battery pack [31–33]. Additionally, some research has been conducted on heat pipes that can manage heat release at a high discharge rate [34]. There are many parameters that affect the performance of the heat pipe, such as the ambient temperature, coolant temperature, coolant flow rate, heat generation rate, start-up time, inclination angle of the heat pipe, and length of the condenser/evaporator section [35].

In our previous study [36], we proposed a new design for heat dissipation in LIB with flat heat pipes coupled with aluminum fins (FHPAF). The overall results indicated that the FHPAF can significantly reduce T_{max} and ΔT_{max}. However, FHPAFs alone cannot handle heat generation at high charge and discharge rates. In this study, cooling performance was enhanced with forced air cooling by an axial fan, and the effect of airflow on the maximum temperature difference of the battery pack (ΔT_{max}) was investigated.

2. Materials and Methods

In this section, the researcher will present details of the battery pack with FHPAF, improvements to the battery cooling system by an axial fan, setting up the equipment used in the experiment, and the experimental method.

2.1. Schematic of the Battery Thermal Management System

In previous work, the battery thermal management system consisted of a copper flat heat pipe with an aluminum fin. A copper flat heat pipe with a sintered copper wick and distilled water as working fluid was chosen. The specification of the flat heat pipe is shown in Table 1.

Table 1. The flat heat pipe specification.

Detail	Value
Type	Flat heat pipe
Material	Copper
Working fluid	Distilled water
Wick	Sintered
Length (mm)	150
Width (mm) × Thickness (mm)	8.0 × 3.0
Operating temperature (°C)	30–120

Aluminum fins (AFs) were installed on the condenser side of the flat heat pipe (FHP) (Figure 2a). The thickness was 2 mm. The width was 3 cm, and the length was 10 cm. The distance between the aluminum fins was 5 cm. One set of FHPAFs consisted of eight FHPs and four aluminum fin plates. There were three sets of FHPAFs, as seen in Figure 2b.

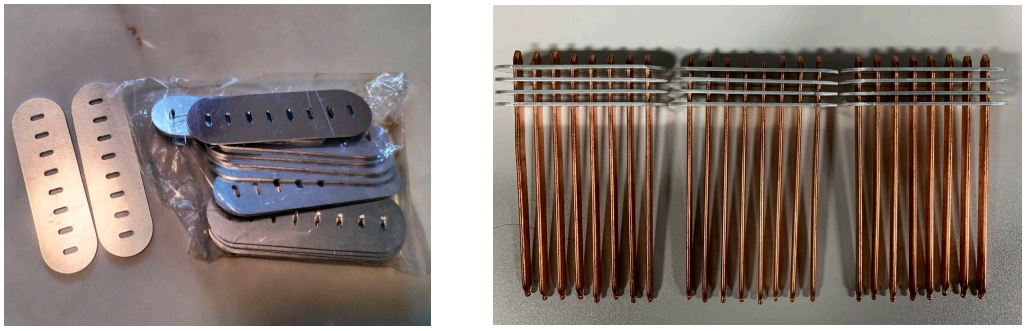

(**a**) (**b**)

Figure 2. Components of the cooling unit: (**a**) aluminum fins; (**b**) three sets of FHPAFs.

The NMC battery pouch cell was used in the experimental tests (Figure 3). The capacity of an NMC cell is 20 Ah per cell. The nominal voltage is 3.7 V. The maximum and minimum voltages are 4.2 V and 2.8 V, respectively. The battery module has seven series-connected pouch cells (7S). Daly brand (Model NMC 7S 24V 100A) was chosen as a battery management system (BMS) to protect the battery pack. The specifications of the battery are presented in Table 2.

Figure 3. The NMC battery pouch cell.

Table 2. The battery cell specification.

Detail	Value
Cathode	NMC
Package	pouch
Capacity (Ah)	20
Nominal voltage (V)	3.7
Maximum voltage (V)	4.2
Minimum voltage (V)	2.5
Internal resistance (mΩ)	1.5
Operating temperature (°C)	−40 to 50
Dimensions H × W × T (mm)	128 × 210 × 7
Weight (kg)	0.345

Three FHPAFs were inserted between the battery cells, as shown in Figure 4b. Thermal grease was filled between the flat heat pipe and aluminum fin and between the battery surface and the heat pipe surface to enhance thermal conductivity [37], as illustrated in Figure 4a.

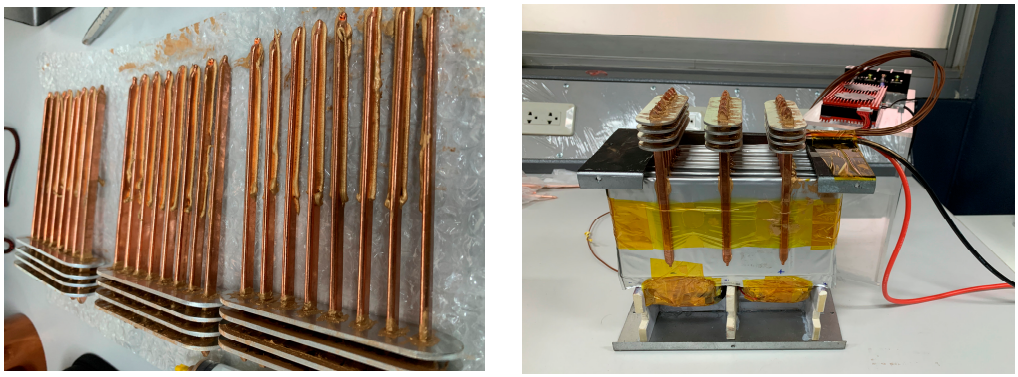

(**a**) (**b**)

Figure 4. Assembling the FHPAFs in the battery pack: (**a**) filling thermal grease; (**b**) installation of FHPAFs.

The battery cells, which were inserted by FHPAFs, were packed in a stainless steel case. The condenser side was placed over the top of the stainless steel case for heat dissipation into the surrounding area. BMS was installed outside the battery pack to prevent heat generated by BMS.

In this study, we enhanced cooling performance with forced air cooling using an axial fan. The rated power of the axial fan was 160 W, and the rated air volume flow rate was 13.3 m^3/min. An acrylic duct was fabricated to control the direction of airflow through the condenser side of the FHP. One side of the acrylic duct was connected with a flexible duct, which connected with an axial fan. The other side was not connected to anything, so that air velocity will be measured on this side. An acrylic duct was installed at the top of the battery pack and sealed with silicone to prevent air leakage. The airflow rate was adjusted using a silicon-controlled rectifier (SCR).

2.2. Experimental Setup

The battery pack was discharged using a bi-directional power supply, IT6005C-80-150 (made by ITECH, Shanghai, China), with a voltage accuracy of 0.01% and a current accuracy of 0.05%. The battery temperature was measured by a K-type thermocouple with an accuracy of 0.1 °C. One thermocouple was attached to the battery surface near the center of the battery. The battery temperature values of seven NMC battery cells were recorded every 2 s using a data logger with eight channels, S220-T8 (made by Huato Electric Co., Ltd., Shenzhen, China), and the temperature was downloaded to a computer.

The air velocity was measured using an anemometer, the Testo 416, with an accuracy reading of 0.2 m/s + 1.5%. Figure 5 shows the image of the experimental setup.

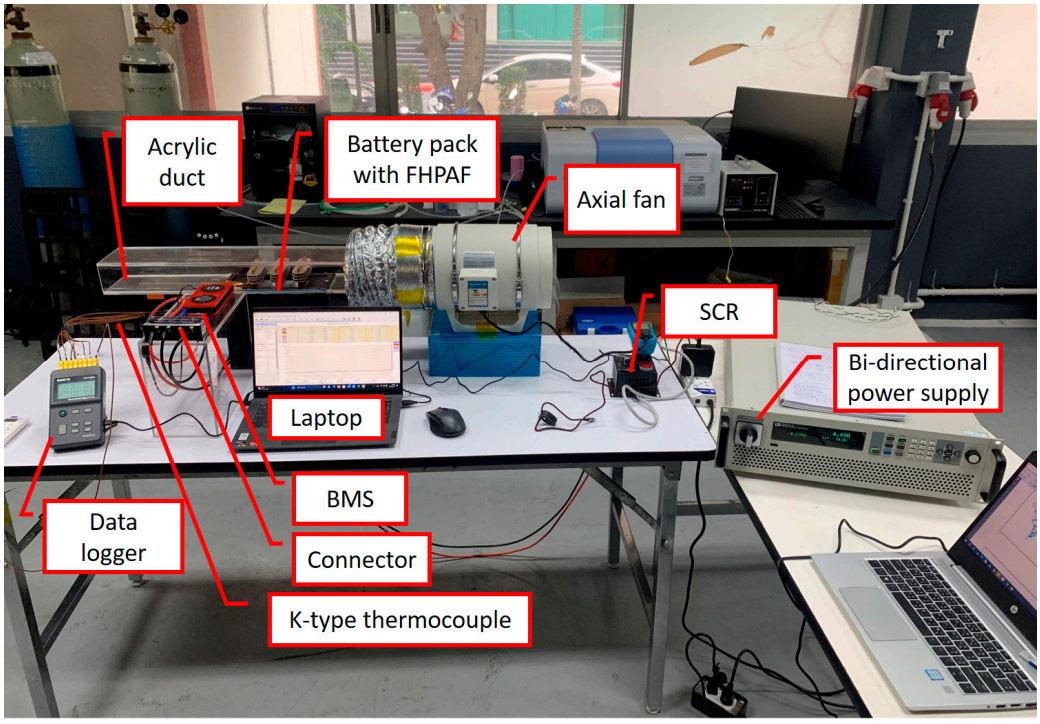

Figure 5. The experimental setup.

2.3. Testing Procedure

To investigate the ΔT_{max}, we discharged the battery pack at room temperature (22–23 °C), and the condenser zone was cooled by means of air under different convection conditions, i.e., natural convection and forced convection, at different air velocity values (12.7 m/s, 9.5 m/s, and 6.3 m/s). The battery cells used in this experiment have a maximum discharge at 6C, and for the safety of the experiment, they were not tested at the maximum capacity of the battery. The battery pack with FHPAFs was discharged at 1C, 2C, 3C, and 4C for all different convection conditions. The charge and discharge rates of a battery are governed by C-rates. The capacity of a battery is commonly rated at 1C, meaning that a fully charged battery rated at 1Ah should provide 1A for one hour. The same battery discharging at 0.5C should provide 500 mA for two hours, and at 2C, it delivers 2A for 30 min. Losses at fast discharges reduce the discharge time, and these losses also affect charge times. In this study, all experiments were tested at discharges of 1C, 2C, 3C, and 4C, so the time for each test was 1 h, 30 min, 20 min, and 15 min, respectively. For protection of the battery cell, the cut-in and cut-off voltages were set at 2.7 V and 4.1 V per cell, or 19.6 V and 28.7 V per battery pack, respectively. Before each test, we charged the battery according to its constant-current mode (CC) and constant-voltage mode (CV). To be specific, the battery was first charged at a constant current of 20 A (i.e., 1C, where C is the rated capacity) until its voltage reached 4.1 V. Charging then proceeded at this constant voltage and finally ended when the battery was fully charged. After charging, the battery pack with FHPAFs was left for a long time to ensure thermal equilibrium with the surroundings at a given room temperature. This was followed by discharging experiments at a constant current, i.e., 20 A (1C), 40 A (2C), 60 A (3C), and 80 A (4C), and seven temperatures on the surface of each battery cell were measured accordingly. The testing procedure flowchart is illustrated in Figure 6.

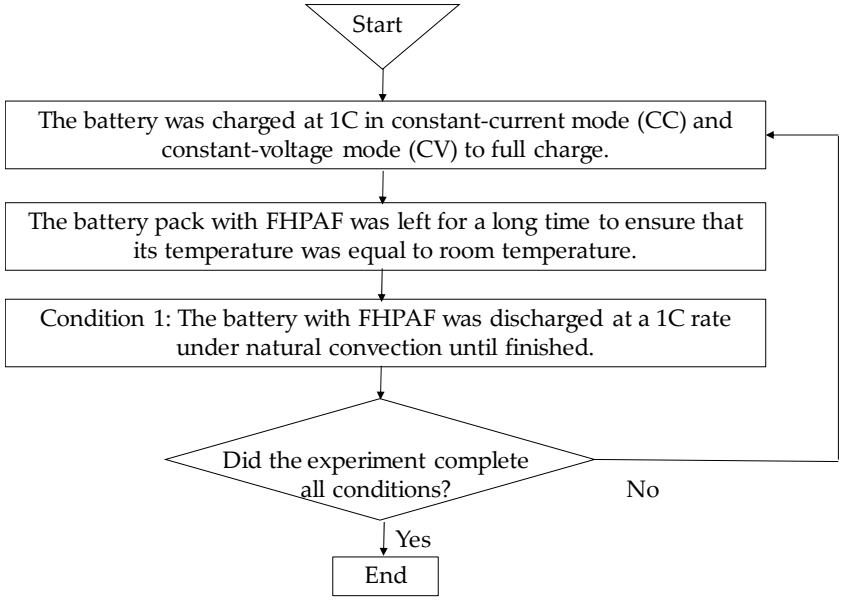

Figure 6. The testing procedure flowchart.

To characterize the thermal responses of the battery in various cooling conditions, we presented the changes in each measured surface temperature, T_i (i = 1, 2,. . ., 7) during the discharge and evaluated their maximum, T_{max}, and maximum differences, ΔT_{max}. These variables are defined, respectively, by

$$T_{max} = \max(T_i) \quad (1)$$

$$\Delta T_{max} = T_{i,max} - T_{i,min} \quad (2)$$

where $T_{i,max,}$ and $T_{i,min}$ represent the maximum and minimum of the seven temperature measurements, respectively. The control criteria are that the $T_{i,max}$ must not exceed 50 °C and the ΔT_{max} must not exceed 5 °C [30]. If the $T_{i,max}$ exceeds 50 °C, the discharge process will be stopped to prevent battery damage.

3. Results and Discussion

The experimental results are included, consisting of air velocity measurements, experimental results at various discharge rates, and a comparison of temperature differences at various rates of discharge in the case where the rate of discharge is constant and the air velocity is constant.

3.1. Air Velocity Measurement

The cross-section dimensions of the acrylic duct were 11 cm in width and 6.5 cm in height. The air velocity was measured using an anemometer, the Testo 416. We conducted the first experiment at 12.7 m/s by adjusting the voltage supply at SCR to 220 V, which was the maximum line-to-neutral voltage. After that, air velocity was reduced by approximately 25% to 9.5 m/s by adjusting the voltage supply at SCR to 145 V. In the last test, air velocity was reduced by approximately 50% to 6.3 m/s by adjusting the voltage supply at SCR to 120 V. Voltage supply cannot reduce it any lower because the T_{max} in Experiment 4C discharge rate was close to 50 °C. If the voltage is lower than this, the T_{max} will be higher than 50 °C, which is the threshold value. The air velocity values were measured at nine points for the purpose of calculating the average value. The air velocity measurement point and air velocity values are shown in Figure 7 and Table 3.

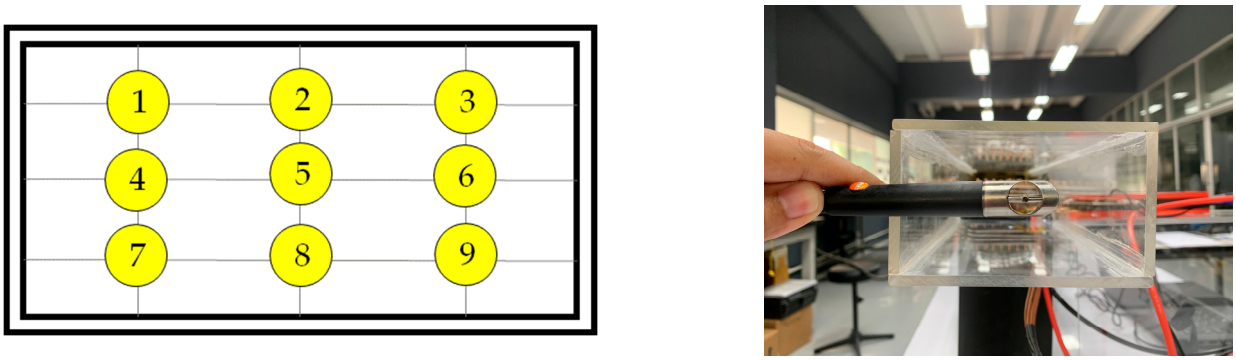

(a) (b)

Figure 7. The air velocity measurement method: (**a**) The air velocity measurement point; (**b**) Air velocity measurement.

Table 3. The air velocity values (the unit of air velocity is m/s).

Point Number	SCR Voltage		
	220 V	145 V	120 V
1	13.2	8.9	5.6
2	11.3	8.0	5.5
3	11.7	8.4	5.4
4	14.0	10.9	7.1
5	10.9	8.3	5.5
6	10.7	6.6	4.3
7	14.3	11.3	7.9
8	14.4	11.1	7.5
9	13.8	11.7	8.2
Average	12.7	9.5	6.3

3.2. Cooling Test at 1C Discharge Rate

At a 1C discharge rate experiment under natural convection, it was found that after 1 h of testing, the highest temperature and the ΔT_{max} occurred at 2780 s, which was T_2, 41.4 °C. The lowest temperature was at 2780 s, which was T_5, 39.0 °C. So, the T_{max} was 41.4 °C, and the ΔT_{max} was 2.4 °C. This result is illustrated in Figure 8a,b.

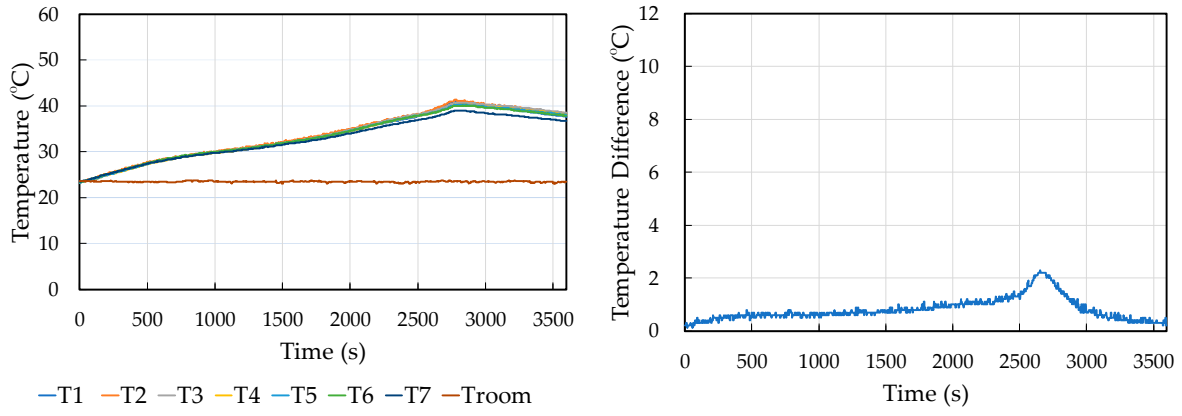

(a) (b)

Figure 8. *Cont.*

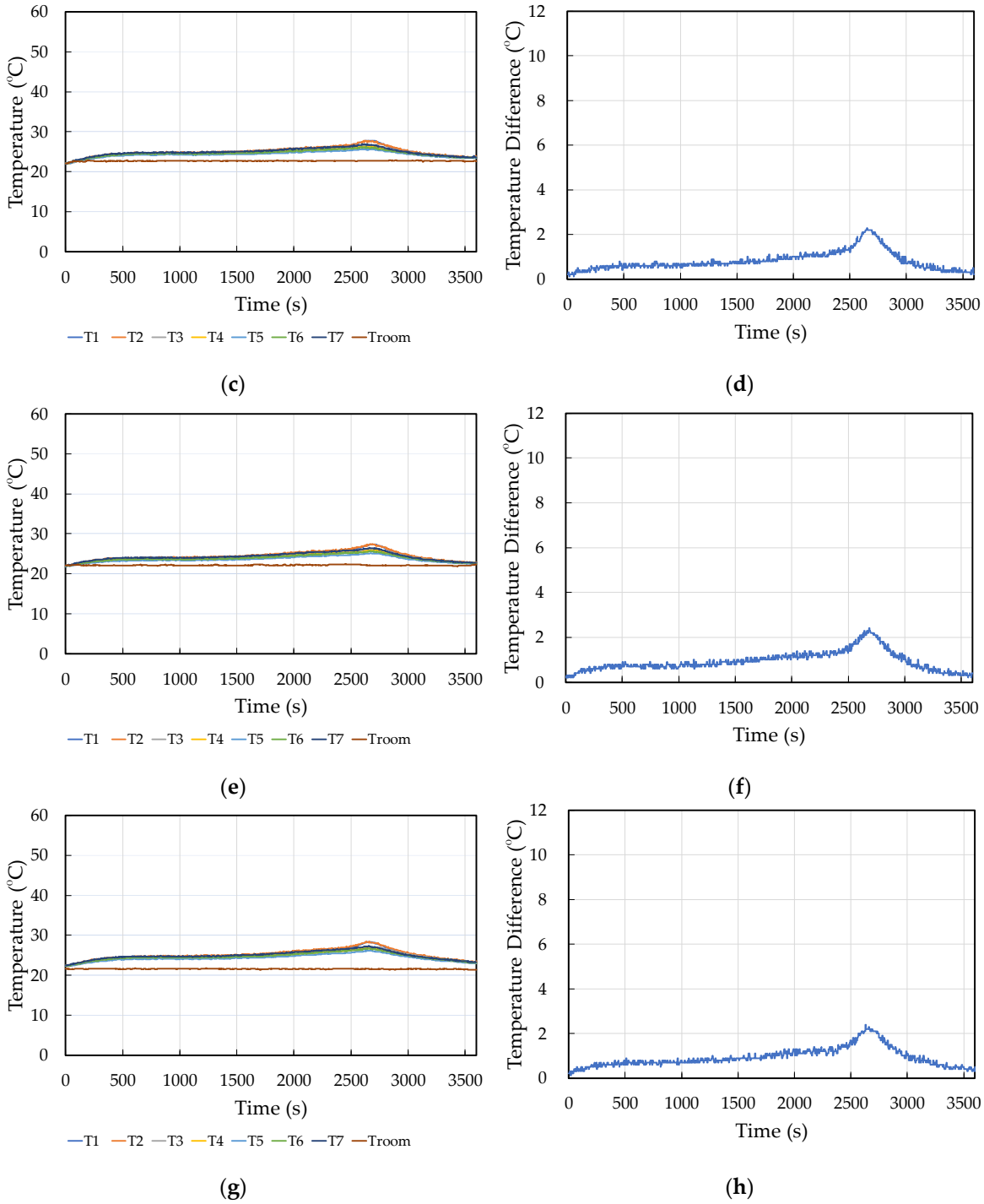

Figure 8. The T_{max} and ΔT_{max} at 1C discharge rate under different convection conditions. (**a**) The T_{max} under natural convection. (**b**) The ΔT_{max} under natural convection. (**c**) The T_{max} under forced convection at an air velocity value of 12.7 m/s. (**d**) The ΔT_{max} under forced convection at an air velocity value of 12.7 m/s. (**e**) The T_{max} under forced convection at an air velocity value of 9.5 m/s. (**f**) The ΔT_{max} under forced convection at an air velocity value of 9.5 m/s. (**g**) The T_{max} under forced convection at an air velocity value of 6.3 m/s. (**h**) The ΔT_{max} under forced convection at an air velocity value of 6.3 m/s.

Under forced convection at an air velocity value of 12.7 m/s, it was found that the highest temperature occurred at 2626 s, which was T_1, 27.8 °C. The lowest temperature was at 2626 s, which was T5, 25.7 °C. At 2626 s, the T_{max} was 27.8 °C and the ΔT was

2.1 °C. However, the ΔT_{max} occurred at 2652 s, which was 2.3 °C. The highest and lowest temperatures were 27.8 °C (T_1) and 25.5 °C (T_5), respectively. This result is illustrated in Figure 8c,d.

Under forced convection at an air velocity value of 9.5 m/s, it was found that the highest temperature occurred at 2668 s, which was T_2, 27.5 °C. The lowest temperature was at 2668 s, which was T_5, 25.2 °C. At 2668 s, the T_{max} was 27.5 °C and the ΔT was 2.3 °C. However, the ΔT_{max} occurred at 2686 s, which was 2.4 °C. The highest and lowest temperatures were 27.5 °C (T_2) and 25.1 °C (T_5), respectively. This result is illustrated in Figure 8e,f.

Under forced convection at an air velocity value of 6.3 m/s, it was found that the highest temperature and the ΔT_{max} occurred at 2630 s, which was T_2, 28.4 °C. The lowest temperature was at 2630 s, which was T_5, 26.0 °C. So, the T_{max} was 28.4 °C, and the ΔT_{max} was 2.4 °C. This result is illustrated in Figure 8g,h.

3.3. Cooling Test at 2C Discharge Rate

At a 2C discharge rate experiment under natural convection, it was found that the temperature of T_1 reached 50.1 °C after discharge proceeded at 1156 s, while the finished time of 2C equals 30 min or 1800 s. The bi-directional power supply was turned off to protect the battery from heat generation. At 1156 s of testing, the highest temperature was 50.1 °C, which was T_1. The lowest temperature was 45.0 °C, which was T_7. So, the T_{max} was 50.1 °C, and the ΔT was 5.0 °C. However, the ΔT_{max} occurred at 1150 s, which was 5.1 °C. The highest and lowest temperatures were 49.9 °C (T_1) and 45.2 °C (T_4), respectively. This result is illustrated in Figure 9a,b.

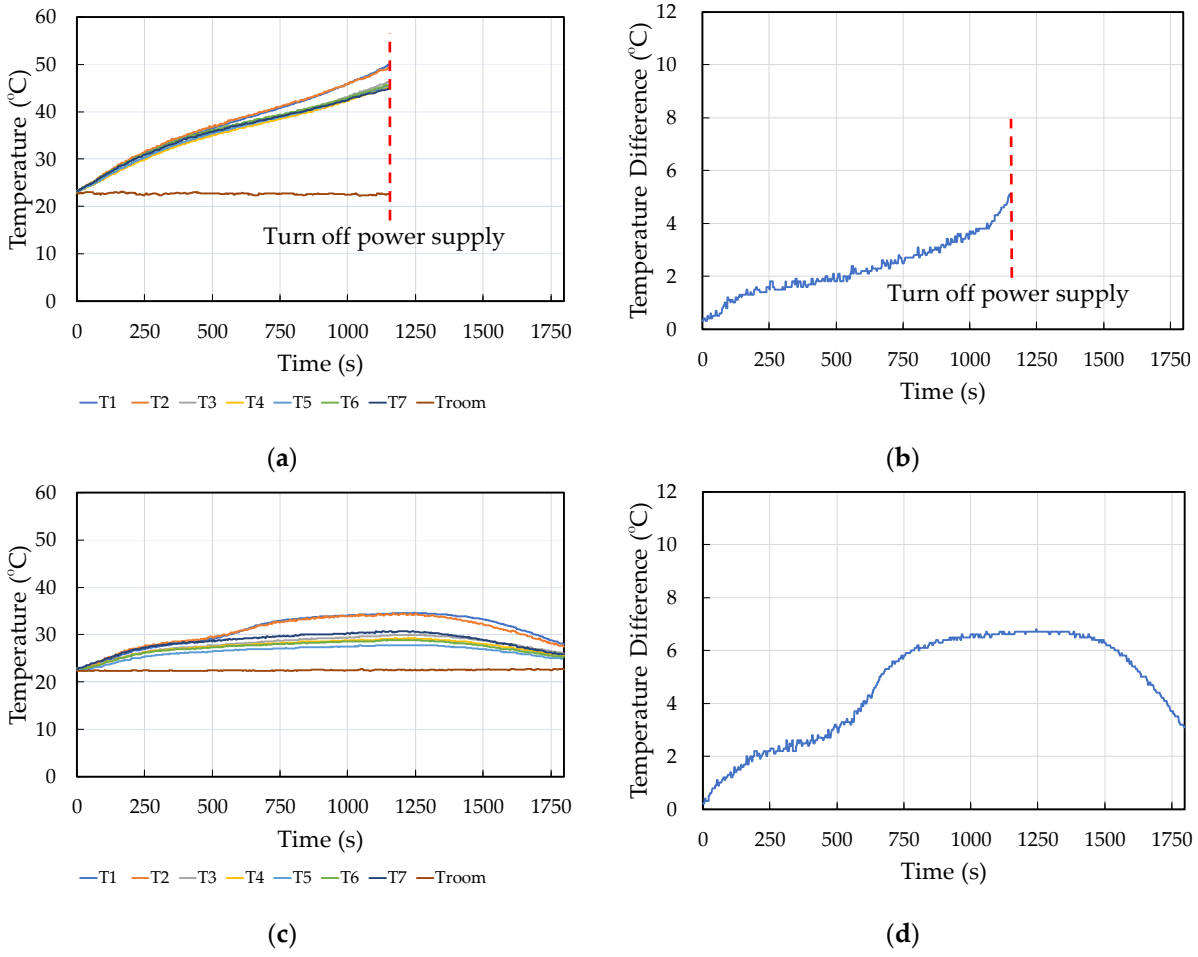

Figure 9. *Cont.*

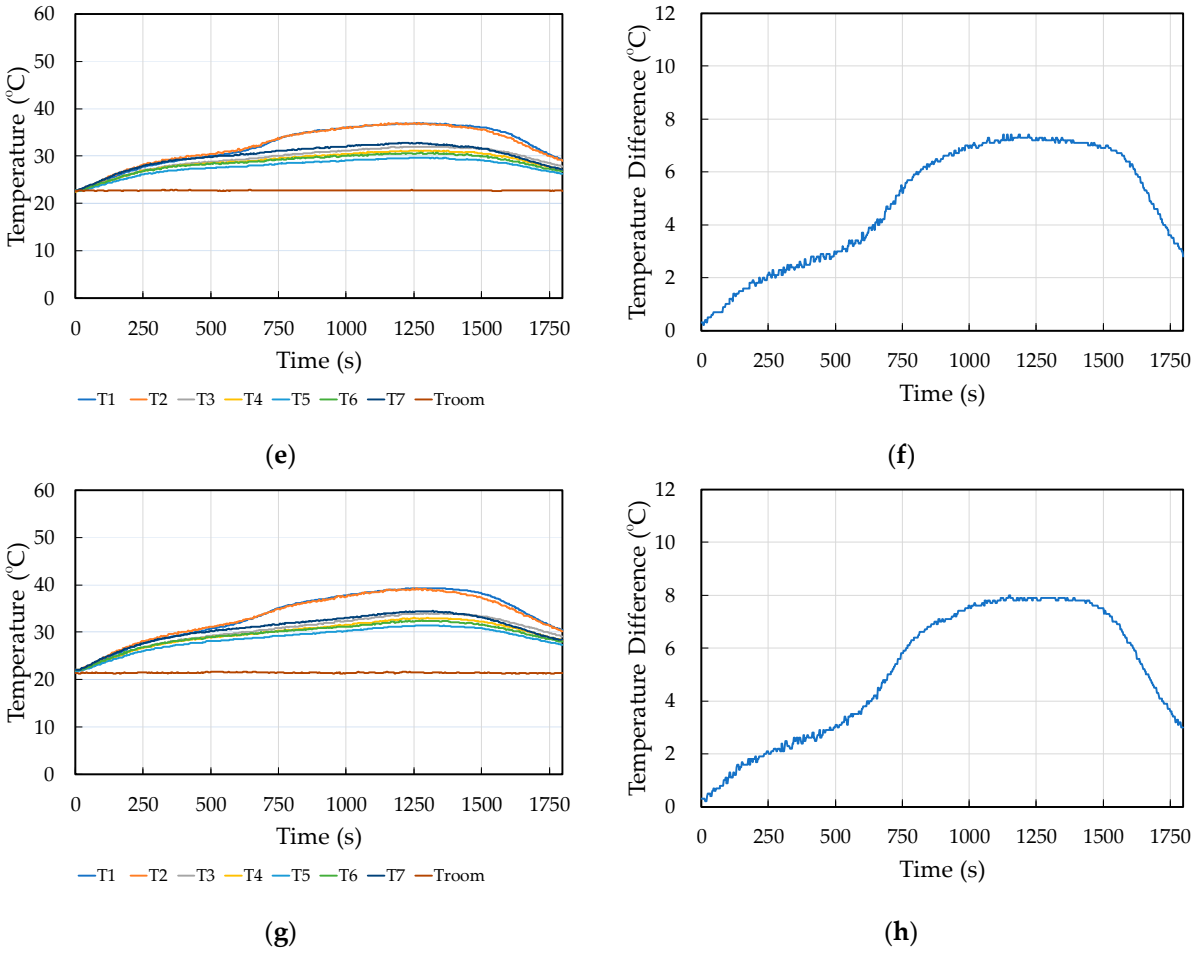

Figure 9. The T_{max} and ΔT_{max} at 2C discharge rate under different convection conditions. (**a**) The T_{max} under natural convection. (**b**) The ΔT_{max} under natural convection. (**c**) The T_{max} under forced convection at an air velocity value of 12.7 m/s. (**d**) The ΔT_{max} under forced convection at an air velocity value of 12.7 m/s. (**e**) The T_{max} under forced convection at an air velocity value of 9.5 m/s. (**f**) The ΔT_{max} under forced convection at an air velocity value of 9.5 m/s. (**g**) The T_{max} under forced convection at an air velocity value of 6.3 m/s. (**h**) The ΔT_{max} under forced convection at an air velocity value of 6.3 m/s.

Under forced convection at an air velocity value of 12.7 m/s, it was found that after 30 min or 1800 s of testing, the highest temperature and the ΔT_{max} occurred at 1246 s, which was T_1, 34.6 °C. The lowest temperature was at 1246 s, which was T_5, 27.8 °C. So, the T_{max} was 34.6 °C, and the ΔT_{max} was 6.8 °C. This result is illustrated in Figure 9c,d.

Under forced convection at an air velocity value of 9.5 m/s, it was found that after 30 min or 1800 s of testing, the highest temperature occurred at 1262 s, which was T_1, 36.9 °C. The lowest temperature was at 1262 s, which was T_5, 29.6 °C. At 1262 s, the T_{max} was 36.9 °C and the ΔT was 7.3 °C. However, the ΔT_{max} occurred at 1128 s, which was 7.4 °C. The highest and lowest temperatures were 36.8 °C (T_2) and 29.4 °C (T_5), respectively. This result is illustrated in Figure 9e,f.

Under forced convection at an air velocity value of 6.3 m/s, it was found that after 30 min or 1800 s of testing, the highest temperature occurred at 1270 s, which was T_1, 39.3 °C. The lowest temperature was at 1262 s, which was T_5, 31.4 °C. At 1270 s, the T_{max} was 39.3 °C and the ΔT was 7.9 °C. However, the ΔT_{max} occurred at 1150 s, which was 8.0 °C. The highest and lowest temperatures were 39.0 °C (T_2) and 31.0 °C (T_5), respectively. This result is illustrated in Figure 9g,h.

3.4. Cooling Test at 3C Discharge Rate

At a 3C discharge rate experiment under natural convection, it was found that the temperature of T_1 reached 50 °C after discharge proceeded for 362 s, while the finished time of 3C equals 20 min or 1200 s. The bi-directional power supply was turned off to protect the battery from heat generation. At 362 s of testing, the highest temperature was 50.0 °C, which was T_1. The lowest temperature was 42.4 °C, which was T_4. So, the T_{max} was 50.0 °C, and the ΔT_{max} was 7.6 °C. This result is illustrated in Figure 10a,b.

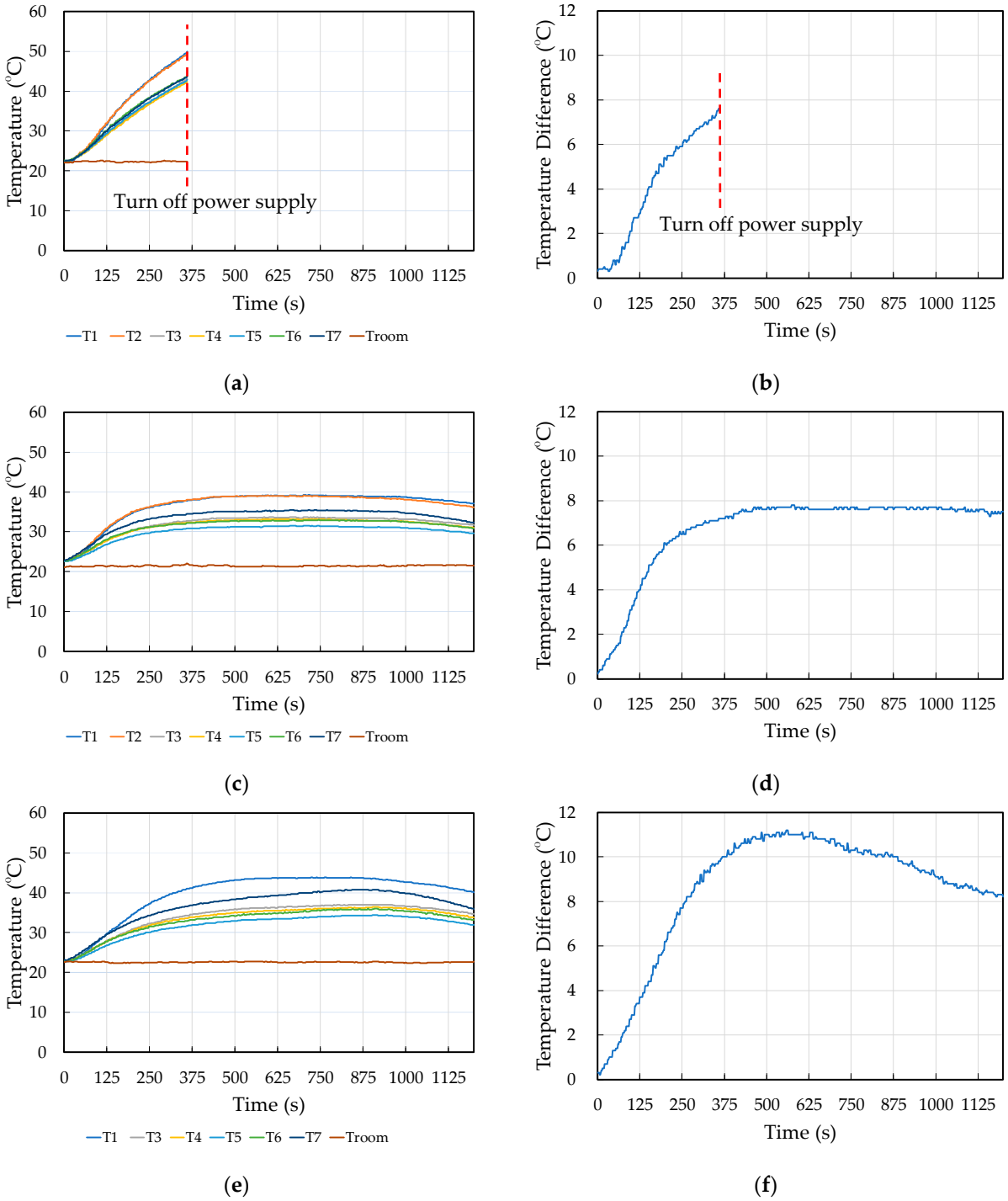

Figure 10. *Cont.*

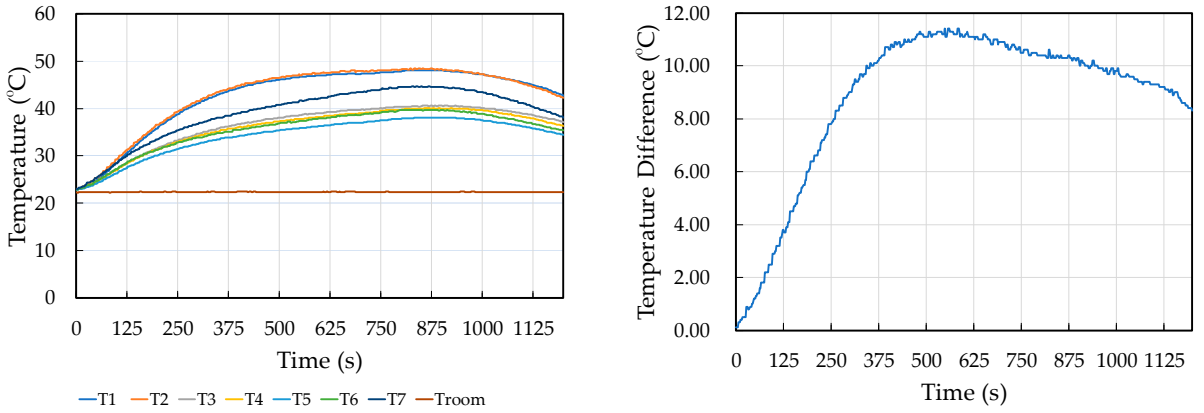

(**g**) (**h**)

Figure 10. The T_{max} and ΔT_{max} at 3C discharge rate under different convection conditions. (**a**) The T_{max} under natural convection. (**b**) The ΔT_{max} under natural convection. (**c**) The T_{max} under forced convection at an air velocity value of 12.7 m/s. (**d**) The ΔT_{max} under forced convection at an air velocity value of 12.7 m/s. (**e**) The T_{max} under forced convection at an air velocity value of 9.5 m/s. (**f**) The ΔT_{max} under forced convection at an air velocity value of 9.5 m/s. (**g**) The T_{max} under forced convection at an air velocity value of 6.3 m/s. (**h**) The ΔT_{max} under forced convection at an air velocity value of 6.3 m/s.

Under forced convection at an air velocity value of 12.7 m/s, it was found that after 20 min or 1200 s of testing, the highest temperature occurred at 702 s, which was T_1, 39.2 °C. The lowest temperature was at 702 s, which was T_5, 31.5 °C. At 702 s, the T_{max} was 39.2 °C and the ΔT was 7.7 °C. However, the ΔT_{max} occurred at 576 s, which was 7.8 °C. The highest and lowest temperatures were 39.0 °C (T_1 and T_2) and 31.2 °C (T_5), respectively. This result is illustrated in Figure 10c,d.

Under forced convection at an air velocity value of 9.5 m/s, it was found that after 20 min or 1200 s of testing, the highest temperature occurred at 630 s, which was T_2, 44.5 °C. The lowest temperature was at 630 s, which was T_5, 33.4 °C. At 630 s, the T_{max} was 44.5 °C, and the ΔT was 11.1 °C. However, the ΔT_{max} occurred at 560 s, which was 11.2 °C. The highest and lowest temperatures were 44.4 °C (T_2) and 33.2 °C (T_5), respectively. This result is illustrated in Figure 10e,f.

Under forced convection at an air velocity value of 6.3 m/s, it was found that after 20 min or 1200 s of testing, the highest temperature occurred at 824 s, which was T2, 48.5 °C. The lowest temperature was at 824 s, which was T_5, 37.9 °C. At 824 s, the T_{max} was 48.5 °C, and the ΔT was 10.6 °C. However, the ΔT_{max} occurred at 550 s, which was 11.4 °C. The highest and lowest temperatures were 47.2 °C (T_2) and 35.8 °C (T_5), respectively. This result is illustrated in Figure 10g,h.

3.5. Cooling Test at 4C Discharge Rate

At a 4C discharge rate experiment under natural convection, it was found that the temperature of T_1 reached 50.2 °C after discharge proceeded for 252 s, while the finished time of 4C equals 15 min or 900 s. The bi-directional power supply was turned off to protect the battery from heat generation. At 252 s of testing, the highest temperature was 50.2 °C, which was T_1. The lowest temperature was 41.8 °C, which was T_4. So, the T_{max} was 50.2 °C, and the ΔT_{max} was 8.4 °C. This result is illustrated in Figure 11a,b.

Under forced convection at an air velocity value of 12.7 m/s, it was found that after 15 min or 900 s of testing, the highest temperature occurred at 520 s, which was T_2, 43.8 °C. The lowest temperature was at 520 s, which was T_4, 35.3 °C. At 520 s, the T_{max} was 43.8 °C, and the ΔT was 10.3 °C. However, the ΔT_{max} occurred at 424 s, which was 10.3 °C. The highest and lowest temperatures were 43.3 °C (T_2) and 33.0 °C (T_4), respectively. This result is illustrated in Figure 11c,d.

Under forced convection at an air velocity value of 9.5 m/s, it was found that after 15 min or 900 s of testing, the highest temperature and the ΔT_{max} occurred at 538 s, which was T_2, 44.3 °C. The lowest temperature occurred at 538 s, which was T_5, 33.2 °C. At 538 s, the T_{max} was 44.3 °C, and the ΔT_{max} was 11.1 °C. This result is illustrated in Figure 11e,f.

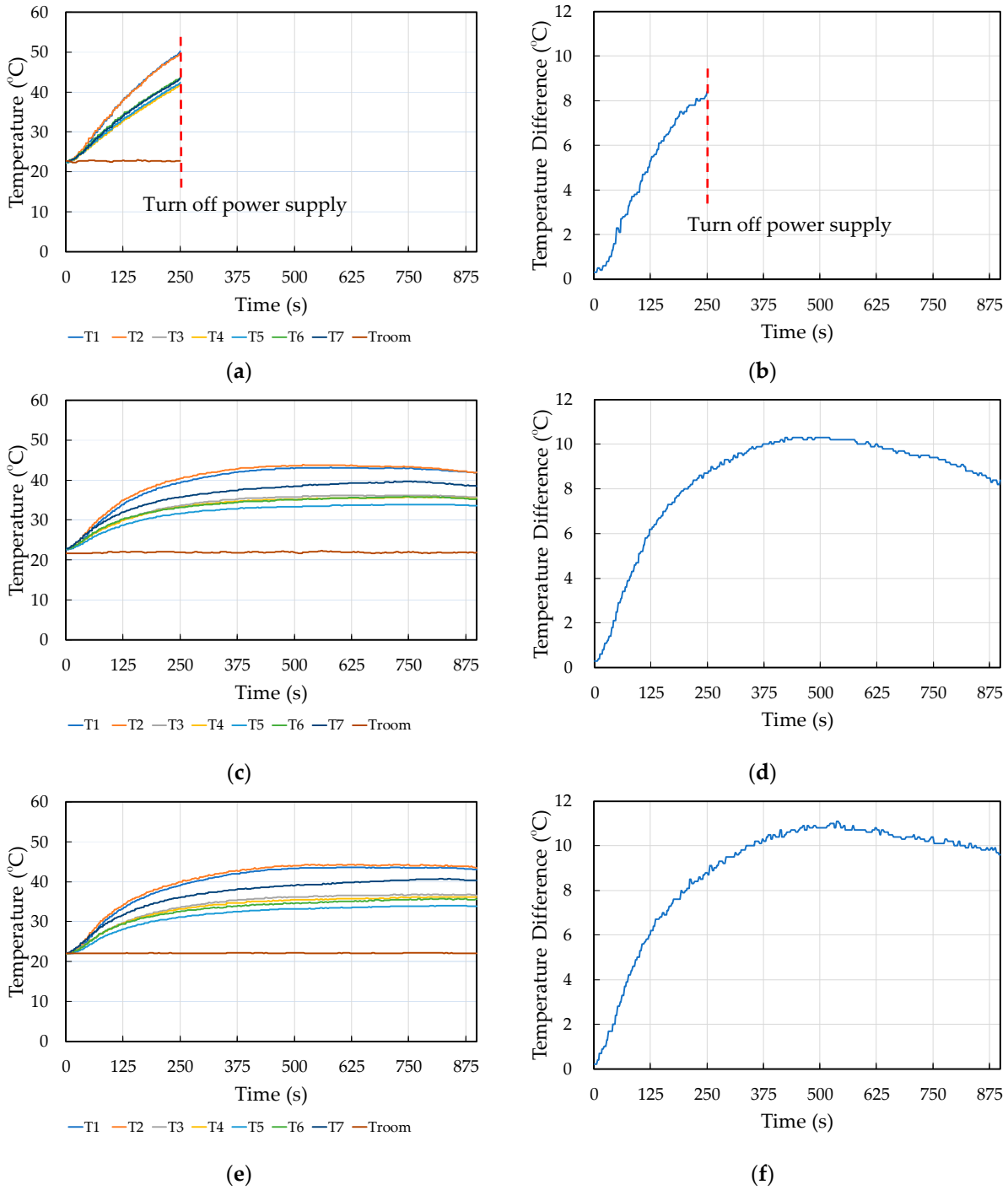

Figure 11. *Cont.*

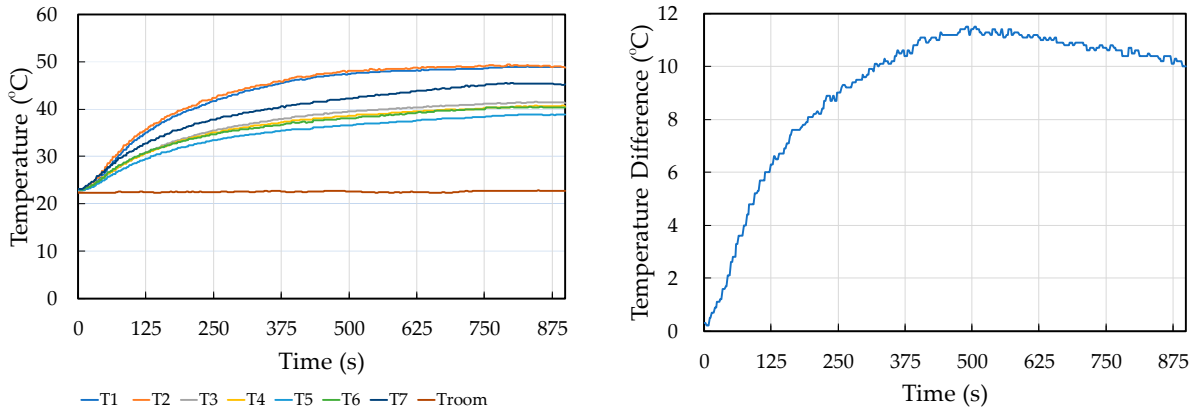

(**g**) (**h**)

Figure 11. The T_{max} and ΔT_{max} at 4C discharge rate under different convection conditions. (**a**) The T_{max} under natural convection. (**b**) The ΔT_{max} under natural convection. (**c**) The T_{max} under forced convection at an air velocity value of 12.7 m/s. (**d**) The ΔT_{max} under forced convection at an air velocity value of 12.7 m/s. (**e**) The T_{max} under forced convection at an air velocity value of 9.5 m/s. (**f**) The ΔT_{max} under forced convection at an air velocity value of 9.5 m/s. (**g**) The T_{max} under forced convection at an air velocity value of 6.3 m/s. (**h**) The ΔT_{max} under forced convection at an air velocity value of 6.3 m/s.

Under forced convection at an air velocity value of 6.3 m/s, it was found that after 15 min or 900 s of testing, the highest temperature occurred at 794 s, which was T_2, 49.4 °C. The lowest temperature was at 794 s, which was T_5, 38.7 °C. At 794 s, the T_{max} was 49.4 °C and the ΔT was 10.7 °C. However, the ΔT_{max} occurred at 490 s, which was 11.5 °C. The highest and lowest temperatures were 48.0 °C (T_2) and 36.5 °C (T_5), respectively. This result is illustrated in Figure 11g,h.

The results of T_{max} and ΔT_{max} of all experiments are summarized in Table 4.

Table 4. The T_{max} and ΔT_{max} values.

Discharge Rate	Parameter	Air Velocity			Natural Convection
		12.7 m/s	9.5 m/s	6.3 m/s	
1C	T_{max} (°C)	27.8	27.5	28.4	41.4
	ΔT_{max} (°C)	2.3	2.4	2.4	2.4
2C	T_{max} (°C)	34.6	36.9	39.3	50.1 *
	ΔT_{max} (°C)	6.8	7.4	8.0	5.1 *
3C	T_{max} (°C)	39.2	44.5	48.5	50.0 *
	ΔT_{max} (°C)	7.8	11.2	11.4	7.6 *
4C	T_{max} (°C)	43.8	44.3	49.4	50.2 *
	ΔT_{max} (°C)	10.3	11.1	11.5	8.4 *

* The discharge process was stopped before the end of the test because the T_{max} exceeded 50 °C.

From all the experimental results in Table 4, it was found that as the discharge rate increased, T_{max} also increased. This was because the higher the discharge rate, the more heat was released from the battery. In addition, it was found that when the discharge rate increased, ΔT_{max} also increased, and ΔT_{max} under natural convection was better than under forced convection because of the turbulence created during forced convection; each battery cell temperature distribution was not uniform. However, if only the case of forced convection were considered, it was found that increasing the air velocity caused the ΔT_{max} to decrease.

3.6. Comparison of the Air Velocity with Discharge Rate

Considering the forced convection condition at any value, it was found that if the discharge rate increased, the ΔT_{max} also increased. At an air velocity of 6.3 m/s, the ΔT_{max} at 1C, 2C, 3C, and 4C discharge rates were 2.4 °C, 8.0 °C, 11.4 °C, and 11.5 °C, respectively. At an air velocity of 9.5 m/s, the ΔT_{max} at 1C, 2C, 3C, and 4C discharge rates were 2.4 °C, 7.4 °C, 11.2 °C, and 11.1 °C, respectively. At an air velocity of 12.7 m/s, the ΔT_{max} at 1C, 2C, 3C, and 4C discharge rates were 2.3 °C, 6.8 °C, 7.8 °C, and 10.3 °C, respectively. This result is illustrated in Figure 12.

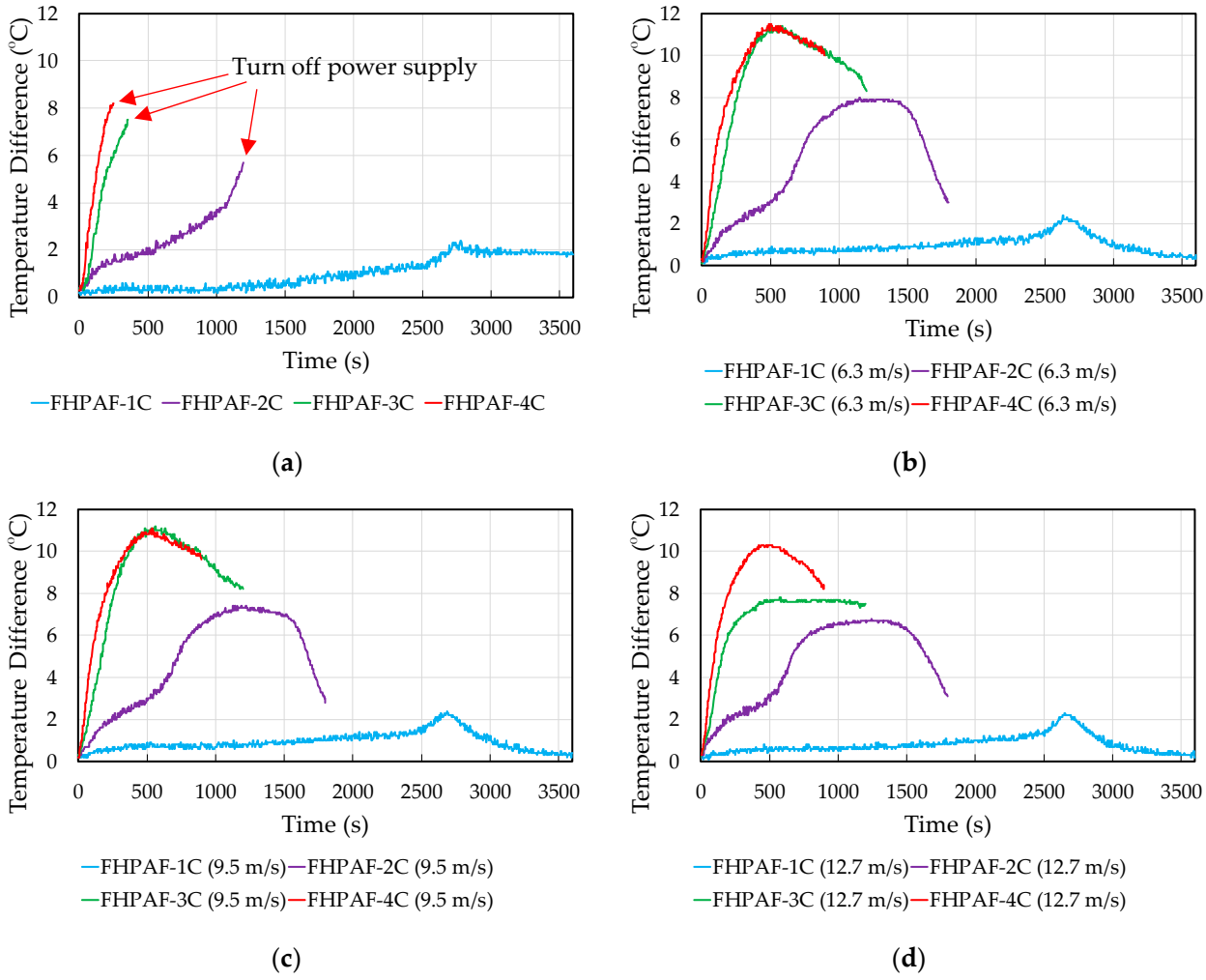

Figure 12. The ΔT_{max} at different convection conditions and various discharge rates. (**a**) The ΔT_{max} under natural convection. (**b**) The ΔT_{max} under forced convection at an air velocity value of 6.3 m/s. (**c**) The ΔT_{max} under forced convection at an air velocity value of 9.5 m/s. (**d**) The ΔT_{max} under forced convection at an air velocity value of 12.7 m/s.

In addition, considering the comparative experimental results with and without forced air convection, it was found that using forced air convection improved the T_{max} significantly. On the other hand, the ΔT_{max} did not improve. In a 1C discharge rete, ΔT_{max} was similar. The ΔT_{max} of the 1C discharge rate without forced convection was 2.4 °C, which equaled the ΔT_{max} at air velocities of 6.3 m/s and 9.5 m/s. The ΔT_{max} at an air velocity of 12.7 m/s was 2.3 °C, which was a little better than 2.4 °C. On the other hand, discharge rates at 2C, 3C, and 4C, ΔT_{max}, were worse than in experiments without forced convection. However, if only the experiments with forced convection were compared, it was found that if the air velocity increased, the ΔT_{max} improved. This result is illustrated in Figure 13.

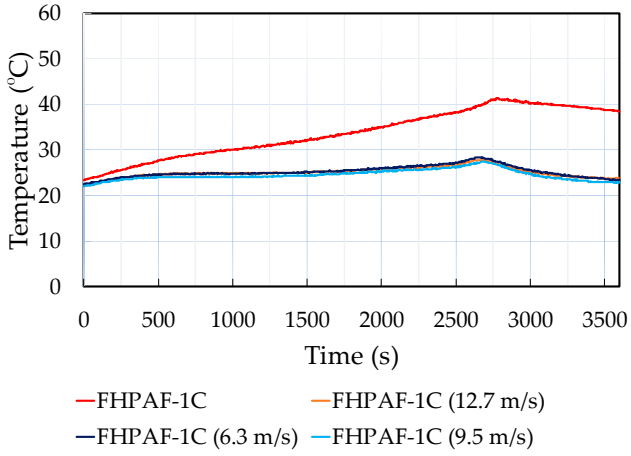

(a)

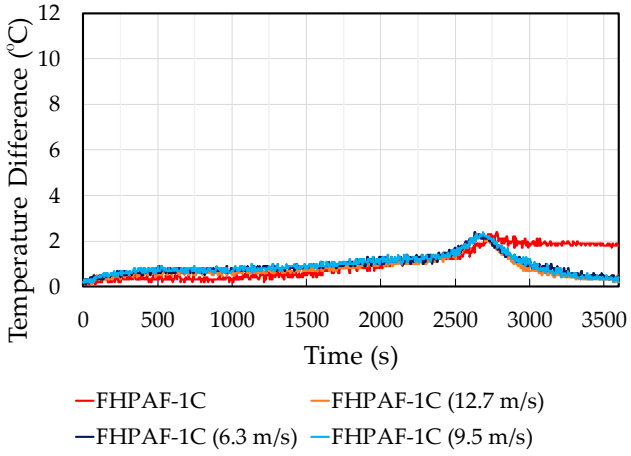

(b)

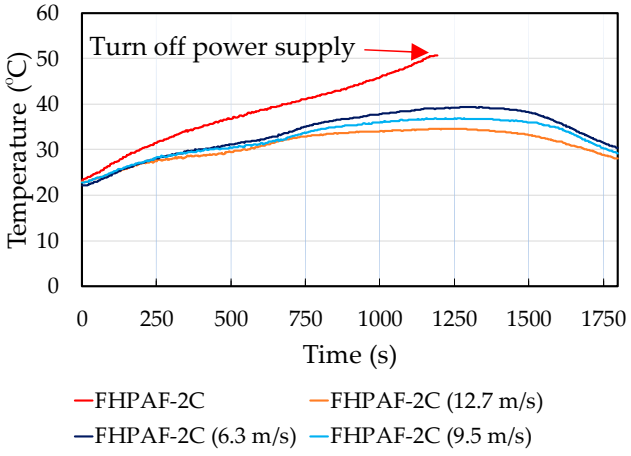

(c)

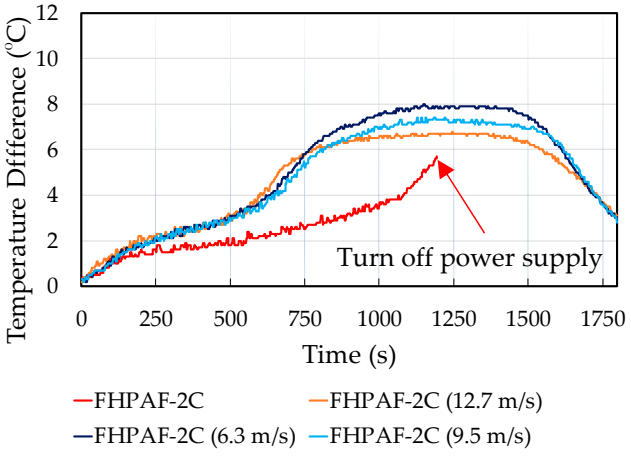

(d)

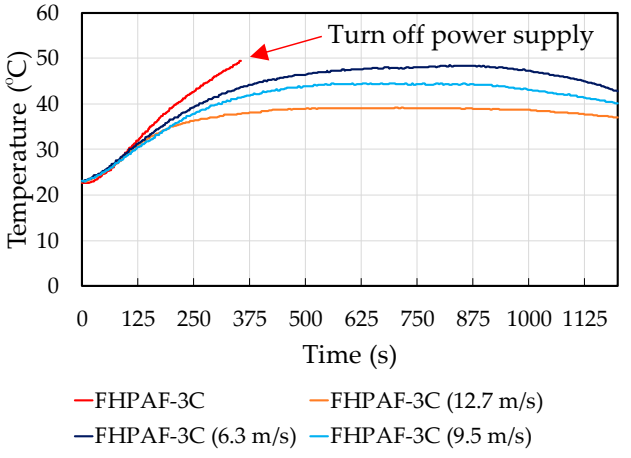

(e)

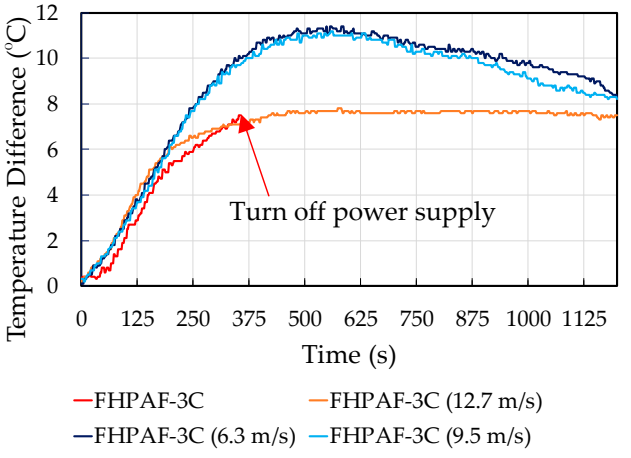

(f)

Figure 13. *Cont.*

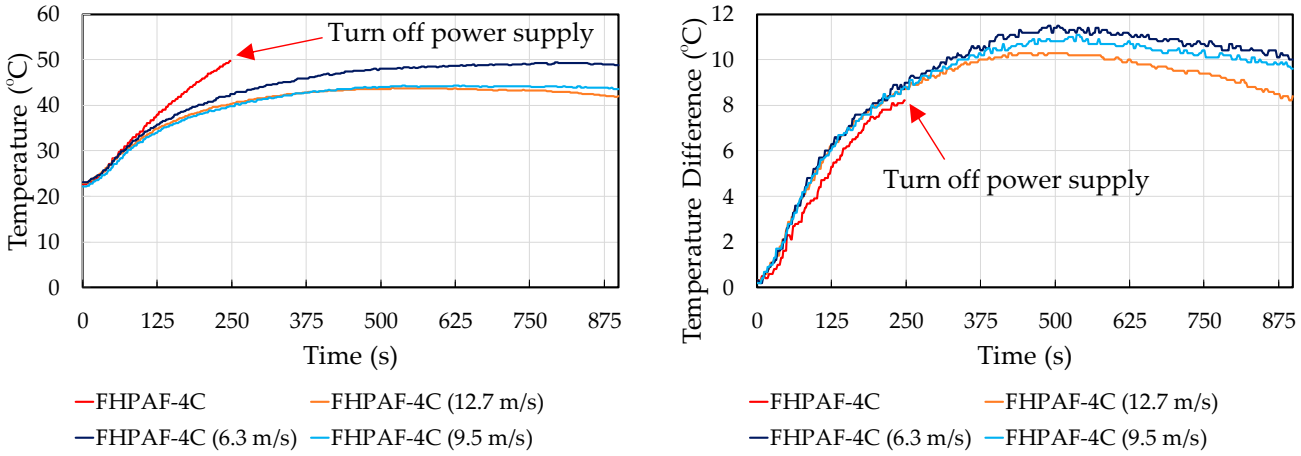

(**g**) (**h**)

Figure 13. The T_{max} and ΔT_{max} at various discharge rates and different convection conditions. (**a**) The T_{max} at 1C discharge rate. (**b**) The ΔT_{max} at 1C discharge rate. (**c**) The T_{max} at 2C discharge rate. (**d**) The ΔT_{max} at 2C discharge rate. (**e**) The T_{max} at 3C discharge rate. (**f**) The ΔT_{max} at 3C discharge rate. (**g**) The T_{max} at 4C discharge rate. (**h**) The ΔT_{max} at 4C discharge rate.

4. Conclusions and Future Work

4.1. Conclusions

In this study, the enhancement in cooling performance using FHPAFs with forced air cooling using an axial fan is presented. The effect of air velocity on the maximum temperature difference of the battery pack (ΔT_{max}) is investigated. The NMC pouch battery cells, 20 Ah in seven series connections, were used in this experiment. All experiments were performed at room temperature under different convection conditions, i.e., natural convection and forced convection, at different air velocity values (12.7 m/s, 9.5 m/s, and 6.3 m/s), with 1C, 2C, 3C, and 4C discharge rates. The results are indicated as follows:

- By increasing the discharge rate while the air velocity remains constant, the ΔT_{max} increases significantly. This is due to the increased heat generated by higher levels of discharging, resulting in a more uniform temperature between batteries.
- The ΔT_{max} under natural convection is lower than under forced convection. Due to the turbulence that forced cooling created, each battery cell temperature distribution was not uniform.
- In forced convection, increasing the air velocity has the effect of decreasing the ΔT_{max}.

According to the results of most experiments, the temperature difference exceeded 5 °C. To solve this problem, the air velocity must be increased. Because of the experimental results, it can be seen that if the air velocity increases, the temperature difference between the battery cells will decrease. In addition, it may be improved by adding heat-absorbing materials evenly throughout the contact surface, such as graphite film or hot plates, etc.

4.2. Future Work

In future studies, computational fluid dynamics (CFD) simulation software (2023 R2) by Ansys® should be used to analyze and confirm the results of experiments. Using CFD simulation software by Ansys® (Canonsburg, PA, USA), it is possible to determine the appropriate number of heat pipes and aluminum fins, air velocity value, and other factors to improve the cooling performance, especially ΔT_{max}.

Author Contributions: Conceptualization, C.A. and C.S.; methodology, C.A. and C.S.; formal analysis, C.A.; investigation, C.A.; resources, C.A. and C.S.; data curation, C.A.; writing—original draft preparation, C.A.; writing—review and editing, S.O. and C.S.; visualization, C.A.; supervision, S.O. and C.S.; project administration, C.S.; funding acquisition, C.S. All authors have read and agreed to the published version of the manuscript.

Funding: National Research Council of Thailand (NRCT), Bangkok, and the National Science, Research and Innovation Fund (NSRF), and King Mongkut's University of Technology North Bangkok with contract No. KMUTNB-FF-66-35.

Data Availability Statement: The data presented in this study are available on request from the corresponding author.

Acknowledgments: This research and innovation activity was funded by the National Research Council of Thailand (NRCT), Bangkok, the National Science, Research and Innovation Fund (NSRF), and King Mongkut's University of Technology North Bangkok with contract No. KMUTNB-FF-66-35.

Conflicts of Interest: The authors declare no conflict of interest.

References

1. United Nation Climate Change. Available online: https://unfccc.int/event/cop-26?item=1#agenda_documents (accessed on 17 September 2023).
2. Ministry of Foreign Affairs, Kingdom of Thailand. Available online: https://www.mfa.go.th/en/content/cop26-glasgow?page=5d5bd3cb15e39c306002a9ac&menu=5d5bd3cb15e39c306002a9ad (accessed on 17 September 2023).
3. Electric Vehicle Association of Thailand. Available online: http://www.evat.or.th/16803970/evat-directory (accessed on 17 September 2023).
4. Wei-Di, L.; Liang-Cao, Y.; Lei, L.; Qishuo, Y.; De-Zhuang, W.; Meng, L.; Xiao-Lei, S.; Qingfeng, L.; Yang, B.; Ian, G.; et al. Grain boundary re-crystallization and sub-nano regions leading to high plateau figure of merit for Bi_2Te_3 nanoflakes. *Energy Environ. Sci.* **2023**. [CrossRef]
5. Khaleghi, S.; Karimi, D.; Beheshti, S.H.; Hosen, S.; Behi, H.; Berecibar, M.; Van Mierlo, J. Online health diagnosis of lithium-ion batteries based on nonlinear autoregressive neural network. *Appl. Energy* **2021**, *282*, 116159. [CrossRef]
6. Shaofeng, W.; Yanping, Z.; Xiaomin, X.; Jaka, S.; Zongping, S. Adsorption-based synthesis of Co_3O_4/C composite anode for high performance lithium-ion batteries. *Energy* **2017**, *125*, 569–575.
7. Fuqiang, X.; Junling, X.; Qizhong, L.; Qingqing, Z.; Binyun, L.; Lianyi, S.; Junjie, C.; Xiaoyan, S.; Zhipeng, S.; Ching-Ping, W. Progress in niobium-based oxides as anode for fast-charging Li-ion batteries. *Energ. Rev.* **2023**, *2*, 100027.
8. Ianniciello, L.; Biwolé, P.H.; Achard, P. Electric vehicles batteries thermal management systems employing phase change materials. *J. Power Sources* **2018**, *378*, 383–403. [CrossRef]
9. Li, A.; Weng, J.; Yuen, A.C.Y.; Wang, W.; Liu, H.; Lee, E.W.M.; Wang, J.; Kook, S.; Yeoh, G.H. Machine learning assisted advanced battery thermal management system: A state-of-the-art review. *J. Energy Storages* **2023**, *60*, 106688. [CrossRef]
10. Huang, Q.; Li, X.; Zhang, G.; Zhang, J.; He, F.; Li, Y. Experimental investigation of the thermal performance of heat pipe assisted phase change material for battery thermal management system. *Appl. Therm. Eng.* **2018**, *141*, 1092–1100. [CrossRef]
11. Jianing, X.; Chuanyu, S.; Yulong, N.; Chao, L.; Chao, W.; He, Z.; Qingjun, Y.; Fei, F. Fast identification of micro-health parameters for retired batteries based on a simplified P2D model by using Padé approximation. *Batteries* **2023**, *9*, 64.
12. Behi, H.; Karimi, D.; Jaguemont, J.; Gandoman, F.H.; Khaleghi, S.; Van Mierlo, J.; Berecibar, M. Aluminum heat sink assisted air-cooling thermal management system for high current applications in electric vehicles. In Proceedings of the 2020 AEIT International Conference of Electrical and Electronic Technologies for Automotive (AEIT AUTOMOTIVE), Turin, Italy, 18–20 November 2020.
13. Jaewan, K.; Jinwoo, O.; Hoseong, L. Review on battery thermal management system for electric vehicles. *Appl. Therm. Eng.* **2019**, *149*, 192–212.
14. Tao, D.; Guodong, Z.; Yan, R.; Ping, L. Thermal performance of lithium ion battery pack by using cold plate. *Appl. Therm. Eng.* **2019**, *160*, 114088.
15. Mengyao, L.; Xuelai, Z.; Jun, J.; Xiaofeng, X.; Yongyichuan, Z. Research progress on power battery cooling technology for electric vehicles. *J. Energy Storages* **2020**, *27*, 101155.
16. Weixiong, W.; Shuangfeng, W.; Wei, W.; Kai, C.; Sihui, H.; Yongxin, L. A critical review of battery thermal performance and liquid based battery thermal management. *Energy Convers. Manag.* **2019**, *182*, 262–281.
17. Yuanwang, D.; Changling, F.; Jiaqiang, E.; Hao, Z.; Jingwei, C.; Ming, W.; Huichun, Y. Effects of different coolants and cooling strategies on the cooling performance of the power lithium ion battery system: A review. *Appl. Therm. Eng.* **2018**, *142*, 10–29.
18. Yuqian, F.; Yun, B.; Chen, L.; Yanyan, C.; Xiaojun, T.; Shuting, Y. Experimental study on the thermal management performance of air cooling for high energy density cylindrical lithium-ion batteries. *Appl. Therm. Eng.* **2019**, *155*, 96–109.
19. Kai, C.; Weixiong, W.; Fang, Y.; Lin, C.; Shuangfeng, W. Cooling efficiency improvement of air-cooled battery thermal management system through designing the flow pattern. *Energy* **2019**, *167*, 781–790.

20. Liwu, F.; Khodadadi, J.M.; Pesaran, A.A. A parametric study on thermal management of an air-cooled lithium-ion battery module for plug-in hybrid electric vehicles. *J. Power Sources* **2013**, *238*, 301–312.
21. Shixue, W.; Kaixiang, L.; Yuan, T.; Junyao, W.; Yukang, W.; Shan, J. Improved thermal performance of a large laminated lithium-ion power battery by reciprocating air flow. *Appl. Therm. Eng.* **2019**, *152*, 445–454.
22. Shahabeddin, K.M.; Yuwen, Z. Cumulative effects of using pin fin heat sink and porous metal foam on thermal management of lithium-ion batteries. *Appl. Therm. Eng.* **2017**, *118*, 375–384.
23. Pranjali, R.T.; Mahendra, M.G.; Sandeep, S.J. Developments in battery thermal management systems for electric vehicles: A technical review. *J. Energy Storages* **2021**, *35*, 102255.
24. Kai, C.; Junsheng, H.; Mengxuan, S.; Shuangfeng, W.; Wei, W.; Yanlai, Z. Design of battery thermal management system based on phase change material and heat pipe. *Appl. Therm. Eng.* **2021**, *188*, 116665.
25. Zhipeng, Y.; Jiakai, Z.; Weiguo, P. A review of battery thermal management systems about heat pipe and phase change materials. *J. Energy Storages* **2023**, *62*, 106827.
26. Mohammad, A.A.; Hussein, M.M.; Ahmed, G.A.; Ohood, H.K.A.; Enas, T.S.; Ali, R.; Hegazy, R.; Hussam, J.; Olabi, A.G. Thermal management systems based on heat pipes for batteries in EVs/HEVs. *J. Energy Storages* **2022**, *51*, 104384.
27. Wu, M.-S.; Liu, K.; Wang, Y.Y.; Wan, C.C. Heat dissipation design for lithium-ion batteries. *J. Power Sources* **2002**, *109*, 160–166. [CrossRef]
28. Lei, S.; Shi, Y.; Chen, G. Heat-pipe based spray-cooling thermal management system for lithium-ion battery: Experimental study and optimization. *Int. J. Heat Mass Transf.* **2020**, *163*, 120494. [CrossRef]
29. Behi, H.; Ghanbarpour, M.; Behi, M. Investigation of PCM-assisted heat pipe for electronic cooling. *Appl. Therm. Eng.* **2017**, *127*, 1132–1142. [CrossRef]
30. Jiaqiang, E.; Feng, Y.; Wenjie, L.; Bin, Z.; Hongyan, Z.; Kexiang, W.; Jingwei, C.; Hong, Z.; Hao, Z.; Yuanwang, D. Effect analysis on heat dissipation performance enhancement of a lithium-ion-battery pack with heat pipe for central and southern regions in China. *Energy* **2021**, *226*, 120336.
31. Xiaoming, X.; Wei, T.; Jiaqi, F.; Renzheng, L.; Xudong, S. Plate flat heat pipe and liquid-cooled coupled multistage heat dissipation system of Li-ion battery. *Int. J. Energy Res.* **2018**, *43*, 1133–1141.
32. Yueqi, W.; Dan, D.; Yi, X.; Weifeng, L.; Hongqiang, G.; Yangjun, Z. Study on the influence of flat heat pipe structural parameters in battery thermal management system. *Front. Energy Res.* **2022**, *9*, 797664.
33. Wang, Y.; Dan, D.; Zhang, Y.; Qian, Y.; Panchal, S.; Fowler, M.; Li, W.; Tran, M.; Xie, Y. A novel heat dissipation based on flat heat pipe for battery thermal management system. *Int. J. Energy Res.* **2022**, *46*, 15961–15980. [CrossRef]
34. Behi, H.; Behi, M.; Karimi, D.; Jaguemont, J.; Ghanbarpour, M.; Behnia, M.; Berecibar, M.; Mierlo, J.V. Heat pipe air-cooled thermal management system for lithium-ion batteries: High power applications. *Appl. Therm. Eng.* **2021**, *183*, 116240. [CrossRef]
35. Boonma, K.; Patimaporntap, N.; Mbulu, H.; Trinuruk, P.; Ruangjirakit, K.; Laoonual, Y.; Wongwises, S. A review of the parameters affecting a heat pipe thermal management system for lithium-ion batteries. *Energies* **2022**, *15*, 8534. [CrossRef]
36. Chokchai, A.; Soontorn, O.; Chaiyut, S. Experiment Investigation on Cooling Performance of Lithium-ion Battery Thermal Management System using Flat Heat Pipe. In Proceedings of the forth Research, Invention and Innovation Congress (RI2C 2023), Bangkok, Thailand, 24–25 August 2023.
37. Xiaohang, L.; Quangui, G.; Xiangfen, L.; Zechao, T.; Shiwen, L.; Junqing, L.; Libin, K.; Dongfang, Z.; Zhanjun, L. Experimental investigation on a novel phase change material composites coupled with graphite film used for thermal management of lithium-ion batteries. *Renew. Energy* **2020**, *145*, 2046–2055.